Substrate Stiffness Modulates Stemness and Differentiation of Rabbit Corneal Endothelium Through the Paxillin–YAP Pathway

Shuting Liu,[1] Hua Chen,[2] Huatao Xie,[1] Xin Liu,[1] and Mingchang Zhang[1]

[1]Department of Ophthalmology, Union Hospital, Tongji Medical College, Huazhong University of Science and Technology, Wuhan, China
[2]Senior Department of Ophthalmology, The Third Medical Center of PLA General Hospital, Beijing, China

Correspondence: Mingchang Zhang, Department of Ophthalmology, Union Hospital, Tongji Medical College, Huazhong University of Science and Technology, Wuhan 430074, China; mingc_zhang@hust.edu.cn.
Xin Liu, Department of Ophthalmology, Union Hospital, Tongji Medical College, Huazhong University of Science and Technology, Wuhan 430074, China; tjkilo@foxmail.com.

SL and HC contributed equally to this article.

Received: August 9, 2023
Accepted: January 18, 2024
Published: March 11, 2024

Citation: Liu S, Chen H, Xie H, Liu X, Zhang M. Substrate stiffness modulates stemness and differentiation of rabbit corneal endothelium through the paxillin–YAP pathway. *Invest Ophthalmol Vis Sci.* 2024;65(3):15. https://doi.org/10.1167/iovs.65.3.15

Purpose. To explore the role of substrate stiffness and the mechanism beneath corneal endothelial cells' (CECs') stemness maintenance and differentiation.

Methods. CECs were divided into central zone (8 mm trephined boundary) and peripheral zone (8 mm trephined edge with attached limbal). Two zones were analyzed by hematoxylin-eosin staining and scanning electron microscopy for anatomic structure. The elastic modulus of Descemet's membrane (DM) was analyzed by atomic force microscopy. Compressed type I collagen gels with different stiffness were constructed as an in vitro model system to test the role of stiffness on phenotype using cultured rabbit CECs. Cell morphology, expression and intracellular distribution of Yes-associated protein (YAP), differentiation (ZO-1, Na^+/K^+-ATPase), stemness (FOXD3, CD34, Sox2, Oct3/4), and endothelial–mesenchymal transition (EnMT) markers were analyzed by immunofluorescence, quantitative RT-PCR, and Western blot.

Results. The results showed that the peripheral area of rabbit and human DM is softer than the central area ex vivo. Using the biomimetic extracellular matrix collagen gels in vitro model, we then demonstrated that soft substrate weakens the differentiation and EnMT in the culture of CECs. It was further proved by the inhibitor experiment that soft substrate enhances stemness maintenance via inhibition of paxillin–YAP signaling, which was activated on a stiff substrate.

Conclusions. Our findings confirm that substrate stiffness modulates the stemness maintenance and differentiation of CECs and suggest a potential strategy for CEC-based corneal tissue engineering.

Keywords: corneal endothelial cells, progenitor, descemet's membrane, stiffness, stemness, YAP

Descemet's membrane (DM), the specialized basement membrane produced by corneal endothelial cells (CECs), contains a form of extracellular matrix (ECM) that is generated during tissue development through a dynamic and reciprocal, biochemical, and biophysical dialogue and the evolving cellular and protein microenvironment.[1–3] The endothelium is a monolayer of hexagonal cells on the DM that transports water from the stroma into the anterior chamber and maintains corneal transparency.[4] Human corneal endothelium shows different characteristics according to their position in DM.[5] Peripheral area of the human cornea endothelium has an increased cell density and positive telomerase activity compared with the central area.[6–9] Well-documented specific stem cell markers were found in the trabecular meshwork (TM) and the transition zone of the human corneal limbus.[10] It is suggested that stem-like cells may be sequestered in niches at the junctional region where the CECs and the TM come together.[11] Coordinated interactions with soluble factors, other cells, and extracellular matrices define a local biochemical and mechanical niche with complex and dynamic regulation that stem cells sense.[12] For now, it is still unclear how the corneal endothelial progenitors interact with niches.

Yes-associated protein (YAP) and transcriptional coactivator with PDZ-binding motif (TAZ) are two homologous transcriptional coactivators that promote cell proliferation, stem cell maintenance, and tissue homeostasis.[13] YAP and TAZ have been identified as conserved mechanotransducers, reading a very diverse set of mechanical cues, from shear stress to cell shape and extracellular matrix rigidity, and translating them into cell-specific transcriptional programs.[14] Focal adhesions (FAs), the main hub for cell mechanosensing, act as a bridge between integrin–ECM connection and the cytoskeleton.[15,16] Paxillin is a main component of FAs and plays an important role in the transduction of extracellular signals into intracellular responses, triggered by the engagement of integrins with the ECM.[17] YAP has been proved to be regulated by integrin/FAK signaling in progeni-

tor cells.[18,19] Previous studies have shown that when human pluripotent stem cells are cultured on a rigid surface, YAP localizes to the nucleus.[20] In contrast, when cells are cultured on soft substrate or with small-molecule inhibitors of F-actin polymerization, YAP translocates out of the nucleus.[21] Prior studies have demonstrated that the phenotype of human corneal limbal epithelial stem cells is highly dependent upon the mechanical properties of their substrate.[22] For now, limited studies have been made to investigate the specific mechanism of the effects of ECM stiffness on CECs' behavior.

Herein, we sought to understand the mechano-microenvironment mechanism regulating YAP subcellular localization in CECs during stemness maintenance and differentiation. This strategy uncovered the stiffness as a critical mechanical cue that regulated YAP localization during stemness maintenance and differentiation.

Materials and Methods

Histology

For clarifying morphologic characteristics, the tissue samples of rabbit cornea were fixed with 4% paraformaldehyde for 1 hour at 37°C. For paraffin sections, tissues were dehydrated through graded alcohols and embedded in paraffin wax until sectioning (10 µm). Hematoxylin and eosin staining was performed on the paraffin sections for morphologic observation on a Leica DFC550 microscope (DFC550; Leica Microsystems, Wetzlar, Germany). For frozen sections, tissues were embedded in optimal cutting temperature (SAKURA, Otsu, Chiba, Japan) compound, cut into sections (10 µm), and then stored at −80°C. Immunofluorescence staining was performed on the frozen sections.

Immunofluorescence Staining

Immunofluorescence staining was performed on the frozen sections of rabbit cornea, collagen substrate, and dishes with CECs. They were washed in PBS and blocked in PBS supplemented with 10% normal goat serum for 1 hour and 0.1% Triton X-100 for 15 minutes at room temperature. Primary antibodies were incubated overnight and detected by secondary antibodies incubated for 2 hours at room temperature. Frozen tissue sections (5–10 µm thick) were fixed in 2% paraformaldehyde (PFA) for 10 minutes at room temperature and permeated in 0.3% TritonX in PBS for 15 minutes. Immunofluorescence characterization of the rabbit cornea and collagen substrate was performed using antibodies (see Supplementary Table S1 for a list of antibodies). Images were obtained with the A1 HD25/A1R HD25 laser scanning confocal microscope (Nikon, Tokyo, Japan). Data were analyzed using the NIS-Elements and the ImageJ (National Institutes of Health [NIH], Bethesda, MD, USA) software suite, with quantification of expression performed by evaluating pixel intensity for each independent channel and normalized against percentage of average pixel intensity of corresponding control. Representative images were taken from each independent gel or corneal tissue sample for all experiments.

Scanning Electron Microscopy

Tissue samples of rabbit cornea and collagen substrate were fixed overnight at 4°C in 1.5% glutaraldehyde (Electron Microscopy Sciences, Hatfield, PA, USA) in 0.1 M sodium cacodylate buffered solution, pH 7.4. Subsequently, the tissue was rinsed twice with 0.1 M sodium cacodylate-buffered solution and fixed for 1 hour on ice in 1% osmium tetroxide (Electron Microscopy Sciences) in sodium cacodylate buffer. Tissue probes were further washed 2× with sodium cacodylate buffer and dehydrated overnight in 70% ethanol, then in 80% ethanol (10 minutes), 90% ethanol (10 minutes), and 100% ethanol absolute (twice 15 minutes, once 30 minutes). Dehydration of the tissue samples was immediately followed by critical point drying. Samples were mounted on 0.5-in. SEM pin stubs (Agar Scientific, London, UK) covered with conductive carbon discs (Agar Scientific) and then coated with gold palladium. Scanning electron microscopy (SEM) images were acquired on a JEOL JSM-6700F Field Emission Scanning Electron Microscope (JEOL Europe B.V., Tokyo, Japan).

Human and Rabbit Corneal Tissues

Three human corneas unsuitable for transplantation were obtained from the Wuhan Red Cross, as authorized (number: S299), by the Medical Ethics Committee of Tongji Medical College, Huazhong University of Science and Technology. All procedures conformed to the Declaration of Helsinki. New Zealand male rabbits (weighed 2.0–2.5 kg, aged 3–4 months) were used for experiments. To obtain the endothelium and DM, rabbits were euthanized with pentobarbital (200 mg kg^{-1}, intravenous). For DM, the endothelial cells were removed, using a modification of previously reported procedures.[23] Briefly, endothelial cells were removed by placing the corneas in 2.5 mM EDTA in HEPES buffer (pH 7.2) for 30 minutes at 37°C followed by sonication (Crest Ultrasonic Cleaner, Ewing, NJ, USA) at 2 A for 5 minutes. Animal experiments were performed in accordance with the ARVO Statement for the Use of Animals in Ophthalmic and Vision Research on the approval of the Institutional Animal Care and Use Committee at Tongji Medical College.

Cell Isolation and Cultivation

CECs were cultivated as described previously.[24–27] Briefly, DM with CECs was stripped and incubated in 1 mg/mL collagenase type I from *Clostridium histolyticum* (17100017; Gibco, Grand Island, NY, USA) for 16 hours. The clusters of CECs were cultured in Opti-MEM I medium (31985070; Gibco) supplemented with 8% fetal bovine serum (10099141C; Gibco), 200 mg/L calcium chloride (C5670; Sigma-Aldrich, St. Louis, MO, USA), 50 µg/mL BPE (02-104; Upstate, Darmstadt, Germany), 20 µg/mL ascorbic acid (A4544; Sigma-Aldrich), 5 ng/mL human epidermal growth factor (E9644; Sigma-Aldrich), 0.08% chondroitin sulfate (C9819; Sigma-Aldrich), and 50 µg/mL penicillin–streptomycin (15140122; Gibco). After 24 hours, medium was replaced with a serum-free modified embryonic stem cell medium composed of DMEM/F12 (11320033; Gibco) with 10% knockout serum (10828010; Gibco), 4 ng/mL fibroblast growth factor–basic (100-18B; PeproTech, Cranbury, NJ, USA), 5 µg/mL ITS (41400045; Gibco), 10 ng/mL hLIF (LIF1050; Sigma-Aldrich), 100 U/mL penicillin–streptomycin. The medium was changed every other day. All cells used in this study were maintained in a 5% CO_2 incubator at 37°C.[28]

Investigative Ophthalmology & Visual Science

Construction of In Vitro Model

The collagen gel preparation and plastic compression were performed as previously described.[29,30] Plastic-compressed, high-density collagen gels were made by sterile rat–tail type I collagen (2.06 mg/mL protein in 0.6% acetic acid; First Link Ltd., West Midlands, UK), 10× Eagle's Minimum Essential Medium (Invitrogen Ltd., Paisley, UK), and 1 M NaOH at an 8:1:1 volume ratio. The solution was gently mixed and cast into circular molds (2 mL per 1.9 cm^2 Ø wells in 12-well plates) prior to gelling for 60 minutes at 37°C. Collagen gels were then fully compressed under layers of nylon mesh (50 µm mesh size), filter papers, and a fixed load of 64 g, which were removed after 15 minutes at room temperature. The plastic-compressed collagen gels then were washed by PBS for 30 minutes. Substrate softening was performed by applying sterile collagenase type I from *C. histolyticum* (17100017; Thermo Fisher Scientific, Waltham, MA, USA). Briefly, lyophilized collagenase powder was solubilized in PBS at 5×10^{-2} g L^{-1} (1×10^4 activity units L^{-1}, 2 units cm^{-2} h^{-1} of total collagenase activity). The gels were subsequently washed thrice with PBS for 15 minutes on a rocker agitator to remove remaining enzyme and digestion-derived soluble products.

Stiffness Measurements

The corneas attached with acellular DM and the substrates with or without softening were stored in Optisol-GS (Bausch & Lomb Inc., Bridgewater, NJ, USA) at 4°C until atomic force microscopy (AFM) measurements could be performed and the left or right eye from each rabbit was randomly assigned to incubate in Optisol-GS for 24 hours. For the measurement, tissues or substrates were adhered using cyanoacrylate glue in the center of a culture dish. AFM analysis was performed in 1× PBS. Briefly, we prepared samples in a water bath. We determined the modulus from the slope of the circle region on the stress–strain curve ($n = 10$ samples per condition). We chose to use a spherical AFM tip with a radius of approximately 5 microns to minimize the strain field and to ensure that the tip size was larger than that of topographic features observed in the corneal stroma and membranes according to the previous study.[31] Statistical analysis was conducted with NanoScope Analysis software (Bruker Corporation, Billerica, MA, USA).

RNA Extraction and Quantitative RT-PCR

Total RNA of corneal endothelial cells was extracted using TRIzol reagent (9108; TAKARA) according to the manufacturer's protocol and an equal amount of RNA was reverse transcribed to cDNA using the PrimeScript RT Reagent Kit (RR047A; TAKARA). Subsequently, quantitative RT-PCR (qRT-PCR) was performed on the StepOnePlus Real-Time PCR System (Life Technologies, Carlsbad, CA, USA) and with a SYBR Premix Ex Taq Kit (RR420A; TAKARA) according to the manufacturer's instructions. β-Actin was used as the internal control, and the $2^{-\Delta\Delta Ct}$ method was used to evaluate the relative expression of mRNA. See Supplementary Table S2 for the sequences of the primer.

Western Blotting Analysis

CECs were lysed in RIPA Lysis and Extraction Buffer with 1% PMSF Protease Inhibitor extracted. The nuclear and cytoplasmic proteins of YAP were dissociated by the nuclear–cytosol extraction kit (P0027; Beyotime Biotechnology, Wuhan, China). Protein concentration was measured by the BCA protein assay kit (23225; Thermo Fisher Scientific). Membranes were blocked with 5% milk or 5% bovine serum albumin for 1 hour at room temperature. Membranes were then incubated with primary antibodies overnight at 4°C. See Supplementary Table S3 for a list of antibodies. Finally, the protein bands were detected by chemiluminescence using an electrochemiluminescence reagent. SACEs (30 µg) were separated by electrophoresis in sodium dodecyl sulfate–polyacrylamide gel and Invitrogen silver staining. Staining intensities were quantified with ImageJ software (NIH).

Statistical Analysis

Statistical analysis was conducted with SPSS 26.0 software (SPSS, Inc., Chicago, IL, USA). Data were expressed as means of independent experiments ± SEM. In qRT-PCR and Western blotting experiments, statistical significance was analyzed by Student's *t*-test (two-tailed; paired or unpaired as appropriate) for comparison between two groups and by one-way ANOVA for multiple comparisons. A comparison between the substrate stiffness was performed by applying the nonparametric Mann–Whitney test. $P < 0.05$ was taken as the level of significance.

Results

CECs With Higher Stemness but Lower Differentiation Marker Expression Resided in the Periphery of the Cornea

Due to the structural characteristics of the DM, we used SEM for visualization. SEM examination illustrated the ultrastructural characteristics of central and peripheral DM (Fig. 1A). To further study the morphology of the periphery, pictures at higher magnifications (×20,000) were taken of these regions. There was a smooth zone between the peripheral endothelium and TM in rabbit, as shown in Figure 1B. The anterior border of the transition was covered by flattened polygonal cells, which became continuous with the trabecular at the posterior border. At the transition, there was an irregular anterior border formed by the peripheral CECs, followed by remnants of the base of pectinate ligaments and a rapid change into TM architecture (Fig. 1B). To characterize the shape of CECs from central and peripheral cornea (the anatomic demarcation is defined in Supplementary Fig. S1), we performed immunostaining and segmentation analyses of the cornea. In peripheral region, a higher cell density, irregular shapes, and occasional cell clusters were observed. In contrast, cells had a defined hexagonal shape and clusters were barely observed in the center (Fig. 1C).

The CECs from the peripheral region expressed lower mature markers, including ZO-1 and Na^+/K^+-ATPase, as shown by immunostaining (Figs. 1C, 1D) and immunoblot analysis (Figs. 1H, 1I). CECs exhibited high expression of proliferation marker Ki67 on the peripheral zone (Figs. 1E, 1G, 1H, 1J).

Importantly, peripheral area of DM represented the location of cells expressing FOXD3, CD34, Oct3/4, and Sox2, core regulators consensually associated with progenitor cells[27] (Figs. 2A, 2B). In contrast, the cells from the central cornea were negative for stemness markers, indi-

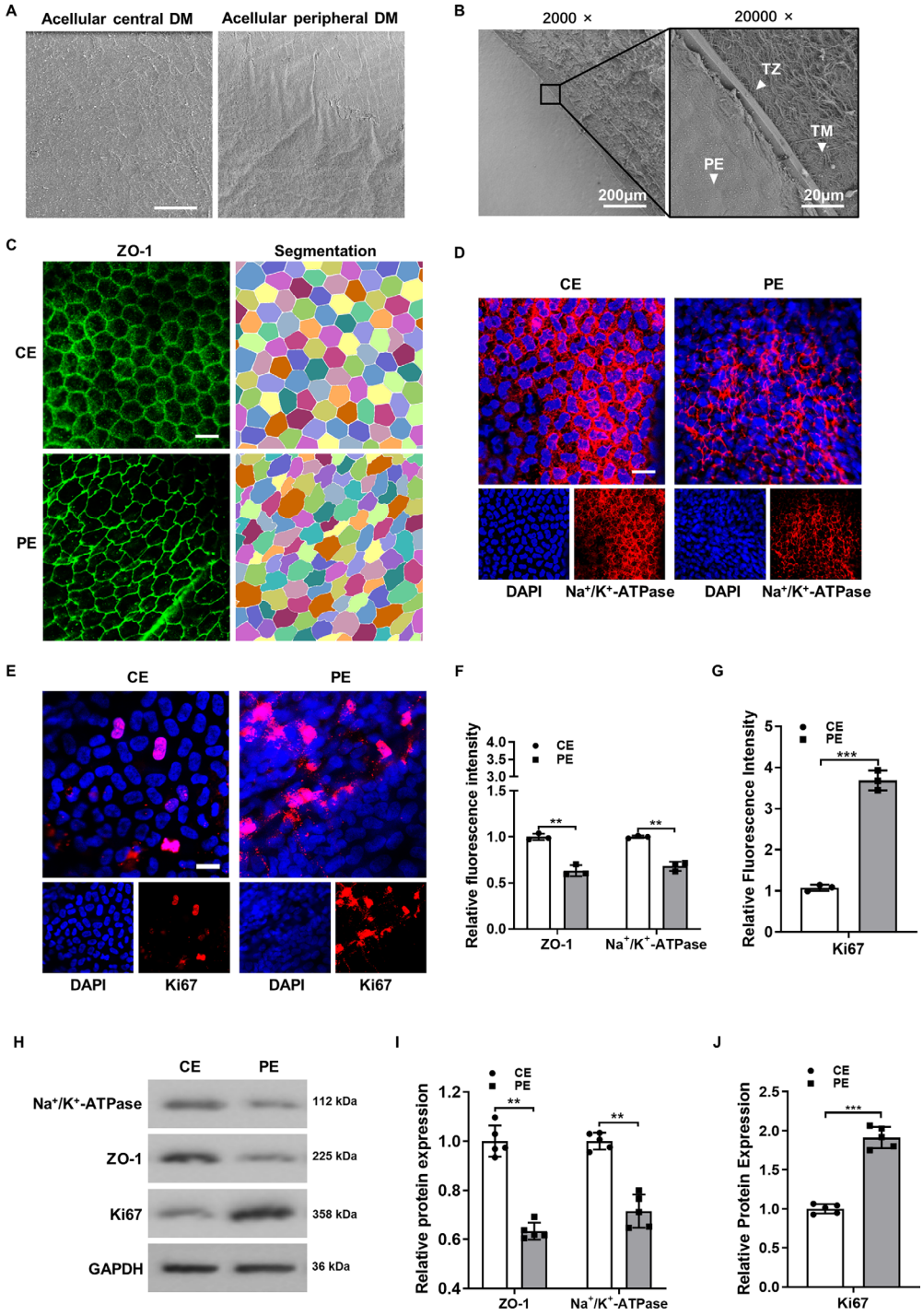

Figure 1. Peripheral endothelium shows lower differentiation but higher proliferation. (**A**) Morphology of Descemet's membrane under scanning electron microscopy. *Scale bar*: 10 μm. (**B**) Morphology of transition zone (TZ) under scanning electron microscopy. *Arrows* refer to peripheral endothelium (PE), transition zone, and trabecular meshwork (TM). *Left scale bar*: 200 μm; *right scale bar*: 20 μm. (**C**) *Left column*: immunostainings of ZO-1 in central (CE) and peripheral (PE) corneal endothelium. *Right column*: Segmentation analyses of the images depicted in the *left column*. *Scale bar*: 20 μm. (**D**) Immunostaining of Na^+/K^+-ATPase in CE and PE. *Scale bar*: 20 μm. (**E**) Immunostaining of Ki67 in CE and PE. *Scale bar*: 20 μm. (**F**, **G**) Relative fluorescence intensity of ZO-1, Na^+/K^+-ATPase, and Ki67 in CE and PE. (**H**, **I**, **J**) Immunoblotting and relative expression of ZO-1, Na^+/K^+-ATPase, and Ki67. Representative images and quantitative data are shown. All quantitative data are presented as mean ± SD. *Bar graphs* show the statistical analysis of at least three independent experiments ($^{**}P < 0.01$ and $^{***}P < 0.001$).

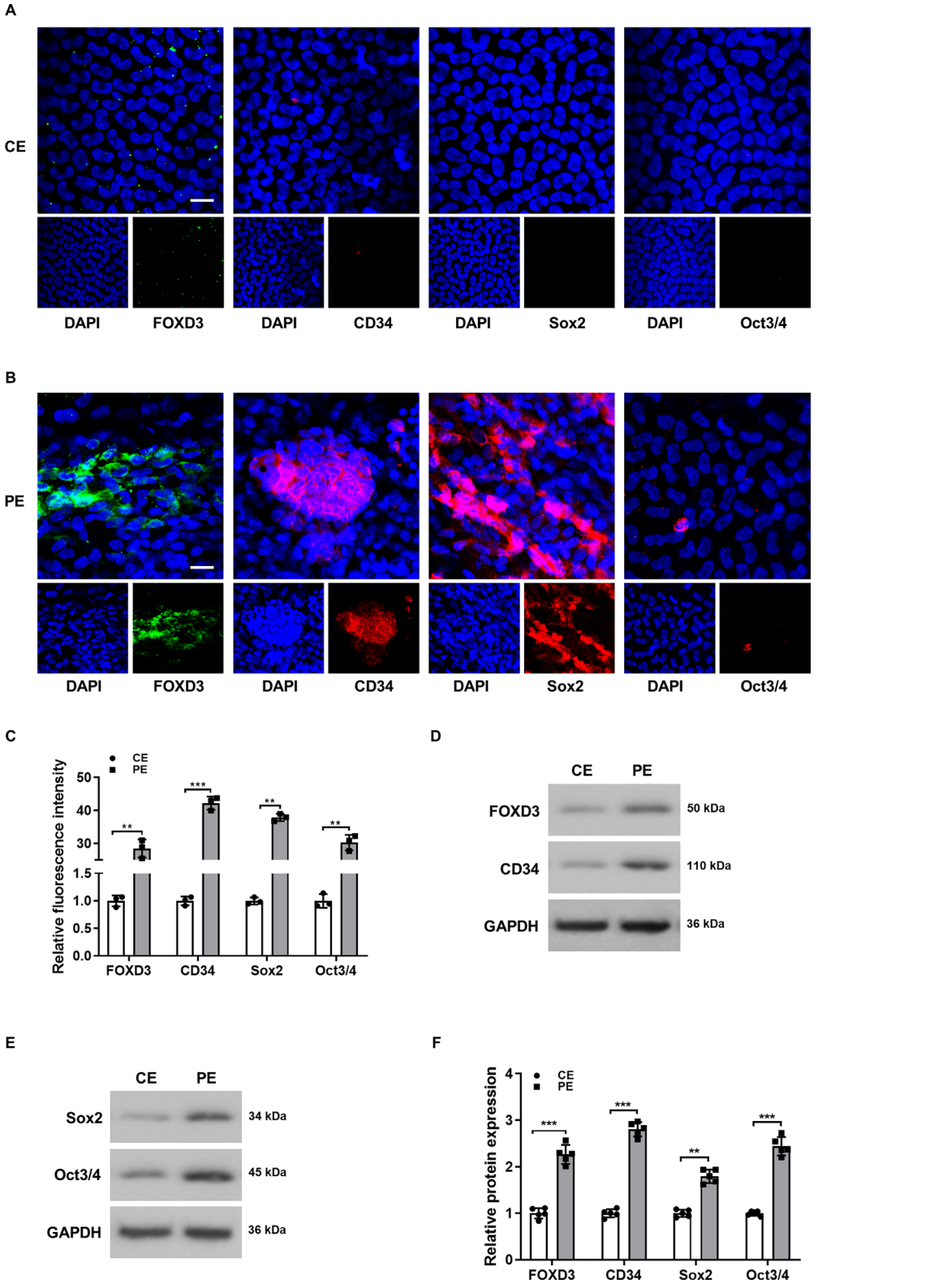

Figure 2. Peripheral endothelium shows higher stemness. (**A**, **B**) Immunostaining of FOXD3, CD34, Sox2, and Oct3/4 in central (**A**) and peripheral (**B**) endothelium. (**C**) Relative fluorescence intensity of FOXD3, CD34, Sox2, and Oct3/4 in central and peripheral endothelium. (**D**, **E**) Immunoblotting of FOXD3 and CD34 (**D**) and Sox2 and Oct3/4 (**E**) in central and peripheral endothelium. (**F**) Relative expression of FOXD3, CD34, Sox2, and Oct3/4 in central and peripheral endothelium. Representative images and quantitative data are shown. All quantitative data are presented as mean ± SD. *Bar graphs* show the statistical analysis of at least three independent experiments (**$P < 0.01$ and ***$P < 0.001$). *Scale bar*: 20 µm in (**A**) and (**B**).

Investigative Ophthalmology & Visual Science

cating that these constituted a more differentiated endothelium (Figs. 2A, 2B). Interestingly, FOXD3 and CD34 tended to be more expressed in cell clusters than in single cells (Fig. 2A). Signal quantification (Fig. 2C) and immunoblot analysis (Figs. 2D–F) also supported the distinctive expression pattern of markers in the peripheral cornea. Collectively, these results indicated that CECs with high stemness but low differentiation marker expression resided in the periphery of the cornea.

YAP Was Inactivated in the Peripheral Zone With Decreased DM Stiffness Ex Vivo

Having revealed the big difference in cell behavior of central and peripheral CECs, we wondered about the contribution of the mechanical microenvironment. In the next study, we focused on stiffness, which refers to a biomechanical property of the ECM, measured as Young's modulus and described in units of pascals (Pa).[31] Acellular DM samples were obtained from New Zealand rabbits. The stiffness of the central area was measured to be 14-fold higher than peripheral area, at 6.88 ± 3.18 kPa, compared to 0.49 ± 0.30 kPa (Fig. 3A). We further validated the stiffness measurement experiment of the central and peripheral parts of the human corneal DM ex vivo. Consistent with what we found in rabbits, the human peripheral DM was softer than the center (64.01 ± 7.01 kPa vs. 38.71 ± 4.73 kPa) (Fig. 3B). In contrast to the central rabbit cornea, cells in the peripheral area showed a significant reduction in YAP expression, in terms of both total expression (tYAP) (Figs. 3C–E) and nuclear location (nYAP) (Figs. 3C, 3D, 3F). Furthermore, we observed minimal nYAP and weak cytoplasmic staining in peripheral cells. In the well-differentiated region, we observed high levels of nYAP (Fig. 3D). Immunoblotting also supported the distinctive expression pattern of markers in the peripheral cornea (Figs. 3G–I).

Taken together, these results showed that corneal endothelial progenitor cells populate tissues that are substantially softer compared to those supporting differentiated CECs, thus constituting niches with distinct biomechanical as well as biochemical/biomolecular profiles.

CECs Presented Higher Stemness But Lower Differentiation on Softer Substrate In Vitro

We thus developed a strategy to investigate the response of progenitor cells to surface compliance, using an in vitro model.

Specifically, we constructed plastic-compressed collagen gels with different stiffness and defined as stiff and soft (Fig. 4A). Elastic moduli of collagen I–coated dish, stiff, and soft substrates were 28.15 ± 4.64 kPa, 5.64 ± 1.36 kPa, and 1.65 ± 1.03 kPa (Fig. 4B).

By SEM, the surface of dish was smooth with no collagen fiber arrangement. The fiber thickness in stiff was similar to soft with no obvious difference in thickness and arrangement (Fig. 4C). After 24 hours, CECs attached on all substrates, but the morphology was of significant diversity. CECs had a smaller and round shape on the soft substrate while presenting a polygonal and larger morphotype on the stiff substrate (Fig. 4D).

At day 7, CECs expressed ZO-1 and Na^+/K^+-ATPase on all substrates (Fig. 4F). On the stiff substrate, CECs presented tighter junctions and higher expression of proliferation and differentiation markers than the soft substrate (Figs. 4E, 4F and Fig. 5C). After CECs reached a state of contact inhibition on day 7, we extended the culture to 14 days for further observation. Under the light microscope morphology, some cells on the dish showed a trend of endothelial–mesenchymal transition (EnMT) (Fig. 4D), accompanied by a decrease in ZO-1 and Na^+/K^+-ATPase expression (Fig. 4G), while the cells on the stiff and soft substrate still maintained a good endothelial cell morphology (Fig. 4D) and stable ZO-1 and Na^+/K^+-ATPase expression (Fig. 4G).

Importantly, we investigated the effects of substrate stiffness on stemness of CECs. The expression of FOXD3, CD34, Sox2, and Oct3/4 was significantly higher on the soft substrate in both immunostaining (Figs. 5A, 5B) and immunoblotting (Fig. 5D) at days 7 and 14.

Collectively, these results confirmed that CECs presented higher stemness but lower differentiation on the softer substrate in the in vitro model.

Substrate Stiffness Mediated the YAP Expression of Corneal Endothelial Cells In Vitro

It has been reported that YAP is regulated by integrin/FAK signaling in progenitor cells. We also observed YAP is inactivated in the peripheral zone with decreased DM stiffness ex vivo. Next, we explored how the stiffness modulates the expression of YAP and its upstream regulator, paxillin, in CECs in vitro. Immunostaining showed no significant difference in intensity of total paxillin between dish, stiff, and soft substrates (Figs. 6A, 6D). We thus analyzed the components of focal adhesions by Western blots (Figs. 6B, 6G). We found that CECs cultured on stiffer substrate showed increased phosphorylation levels of paxillin (Figs. 6A, 6D, 6G). CECs on the soft substrate showed a lower expression and more cytoplasmic localization of YAP compared with those plated on the stiff substrate and dish (Figs. 6A, 6F). Immunoblotting also supported the expression pattern of markers (Figs. 6C, 6E, 6H, 6I).

In summary, these data indicate that substrate stiffness affects the phosphorylation of paxillin and the localization and expression of YAP in CECs.

YAP Inhibitor Restrained the EnMT, Which Was Induced by Substrate Stiffness and Enhanced the Stemness of CECs

CECs on the soft substrate showed a lower total YAP expression but higher cytoplasmic localization compared with those plated on the stiff substrate and dish (Fig. 6C). This was consistent with an ex vivo pattern (Fig. 3G). To further verify that YAP is involved in stiff-induced cell behavior changes in CECs, in a subsequent experiment, the small-molecule YAP inhibitor verteporfin (VP) was added to the stiff substrate at day 6. We found that VP treatment remarkably decreased YAP, TAZ, and TEAD1 expression in a dose-dependent manner (Figs. 7A, 7G). We also found fibrotic proteins markers (vimentin, α-SMA, fibronectin, type I collagens) (Figs. 7B, 7I) related to EnMT were downregulated in a dose-dependent manner. Immunostaining revealed a lower expression and cytoplasmic localization of YAP of CECs on the stiff substrate with 5 µM VP compared with those without any treatment (Fig. 7C). Immunostaining also showed that through 5 µM VP treatment, the EnMT-related marker vimentin of CECs on the stiff matrix could

Investigative Ophthalmology & Visual Science

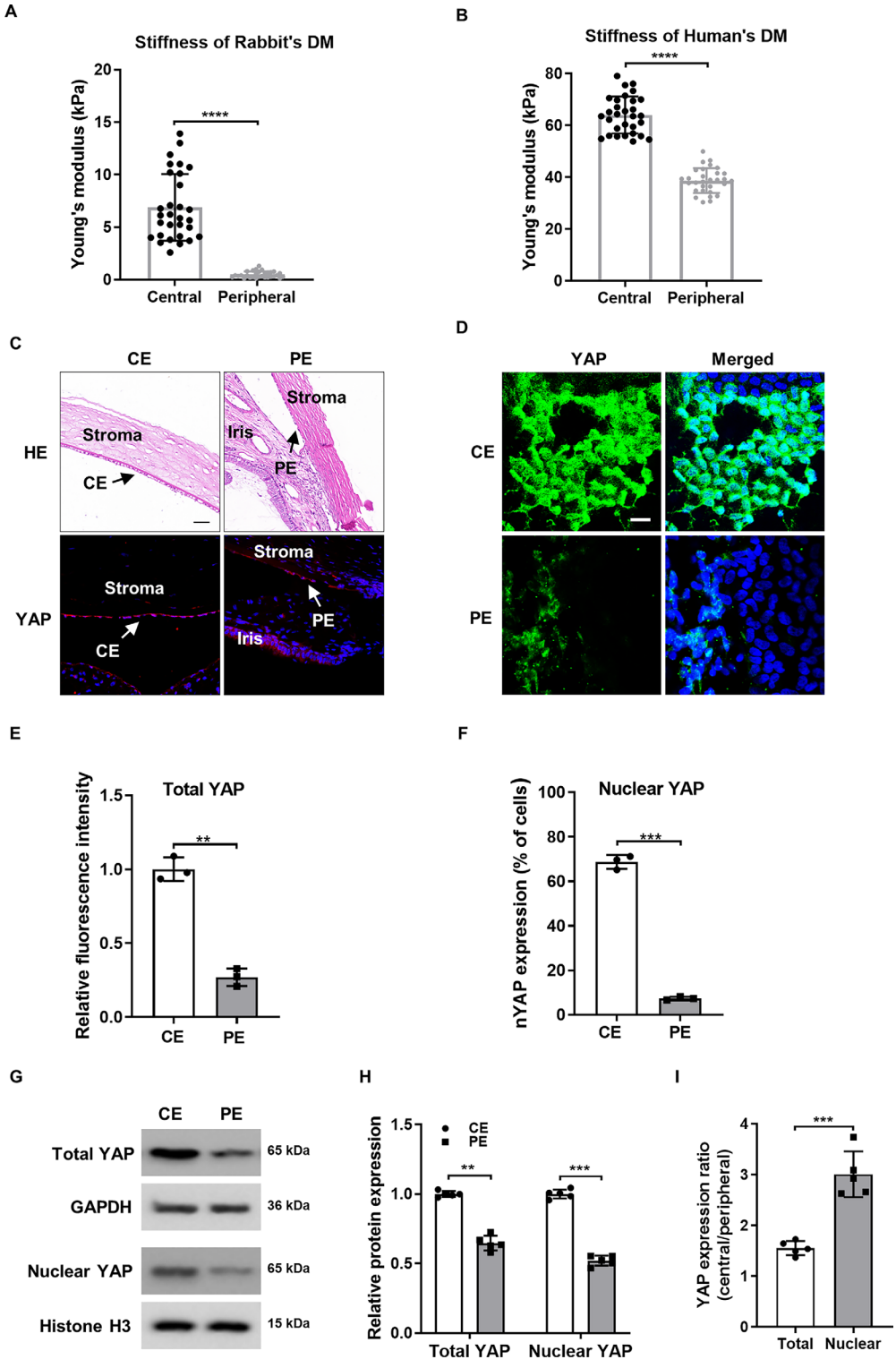

Figure 3. YAP is inactivated in peripheral zone with decreased DM stiffness ex vivo. (**A**, **B**) Elastic modulus (kPa) of central and peripheral Descemet's membrane of rabbit and human calculated from three independent experiments using force–distance spectroscopy ($n = 3$). Indentation points = 10 for each experiment. (**C**) Hematoxylin and eosin staining of cornea and immunostaining of YAP cellular localization in central and peripheral endothelium. (**D**) Immunostaining of YAP in central and peripheral endothelium. (**E**, **F**) Relative fluorescence intensity of total YAP (**E**) and nuclear YAP expression (**F**) of endothelial cells in central and peripheral cornea. (**G**, **H**) Immunoblotting and relative expression of total or nuclear YAP. (**I**) The total YAP expression ratio of central/peripheral cells and the nuclear YAP expression ration of central/peripheral cells. Representative images and quantitative data are shown. *Bar graphs* show the statistical analysis of at least three independent experiments. All quantitative data are presented as mean ± SD ($^{**}P < 0.01$ and $^{***}P < 0.001$). *Scale bar*: 50 µm in (**C**) and 20 µm in (**D**).

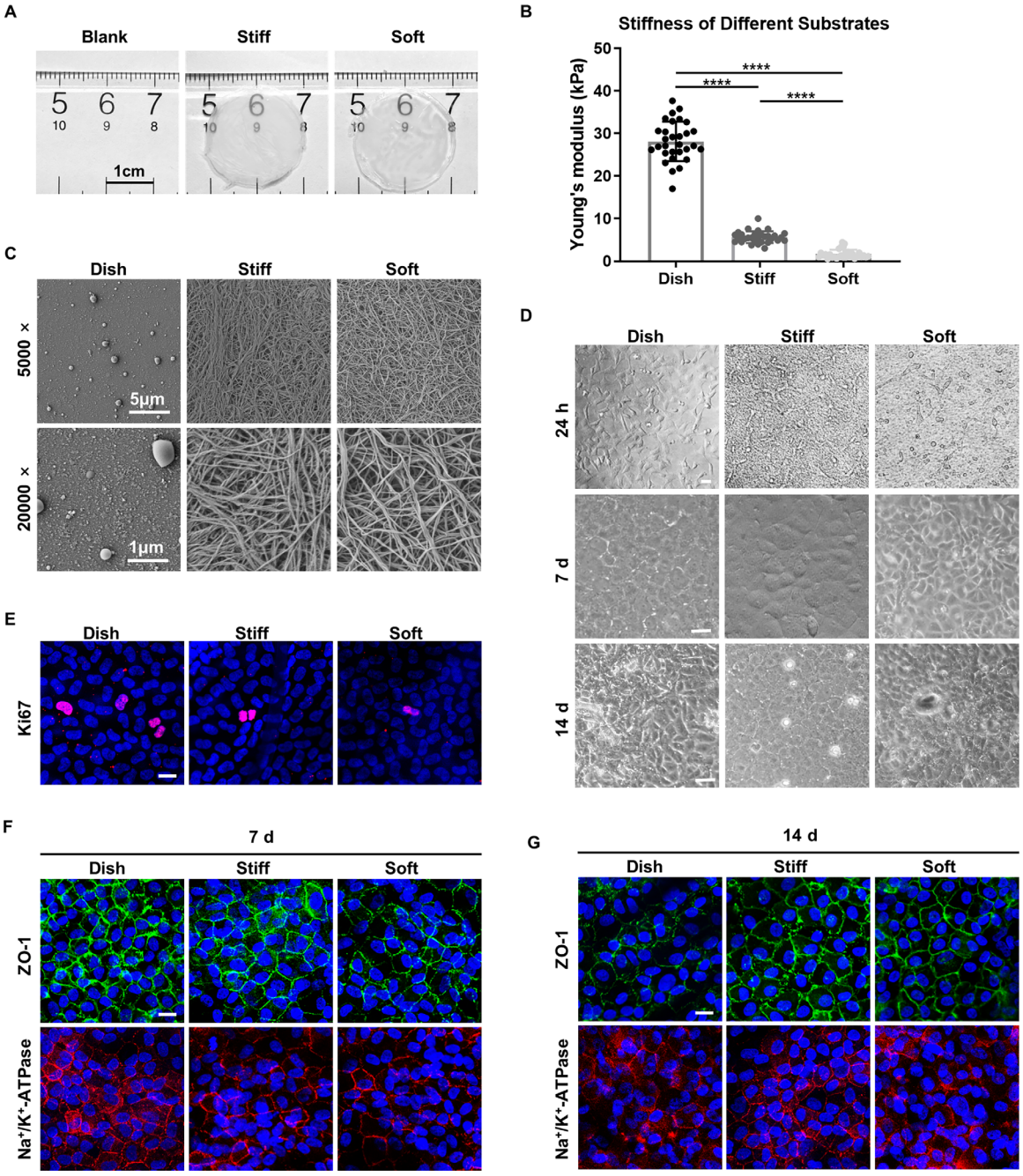

Figure 4. Substrate stiffness regulates the morphology and differentiation of CECs in vitro. (**A**) Stiff and soft substrates made of plastic-compressed collagen gels. (**B**) Elastic modulus (kPa) of dish, stiff, and soft substrates calculated from three independent experiments using force–distance spectroscopy ($n = 3$). Indentation points = 10 for each experiment. (**C**) Morphology of dish, stiff, and soft under scanning electron microscopy. (**D**) Morphology of CECs on dish, stiff, and soft substrates after 24-hour, 7-day, and 14-day culture. (**E**) Immunostaining of Ki67 of CECs in dish, stiff, and soft substrates after 7-day culture. (**F**, **G**) Immunostaining of ZO-1 and Na^+/K^+-ATPase of CECs in dish, stiff, and soft substrates after 7-day culture (**F**) and 14-day culture (**G**). Representative images and quantitative data are shown. *Bar graphs* show the statistical analysis of at least three independent experiments. All quantitative data are presented as mean ± SD (****$P < 0.0001$). *Scale bar*: 1 cm in (**A**), 5 μm in *upper row* of (**C**), 1 μm in *lower row* of (**C**), 20 μm in (**D**), and 20 μm in (**E**), (**F**), and (**G**).

be restored to its expression state on the soft substrate (Fig. 7D). Importantly, although it had no effect on central CECs (Supplementary Fig. S2), the stemness markers (Sox2, Oct3/4, and Nanog) (Figs. 7E, 7H) of peripheral CECs were also upregulated by YAP inhibitor. Of note, we also found that the main content of DM and differentiation marker of CECs (Figs. 7F, 7I), which were elevated on the stiff substrate, were also downregulated by YAP inhibitor in a dose-dependent manner. Therefore, it could be inferred that the substrate stiffness modulates the stemness maintenance, differentiation, and EnMT of CECs through the paxillin–YAP pathway.

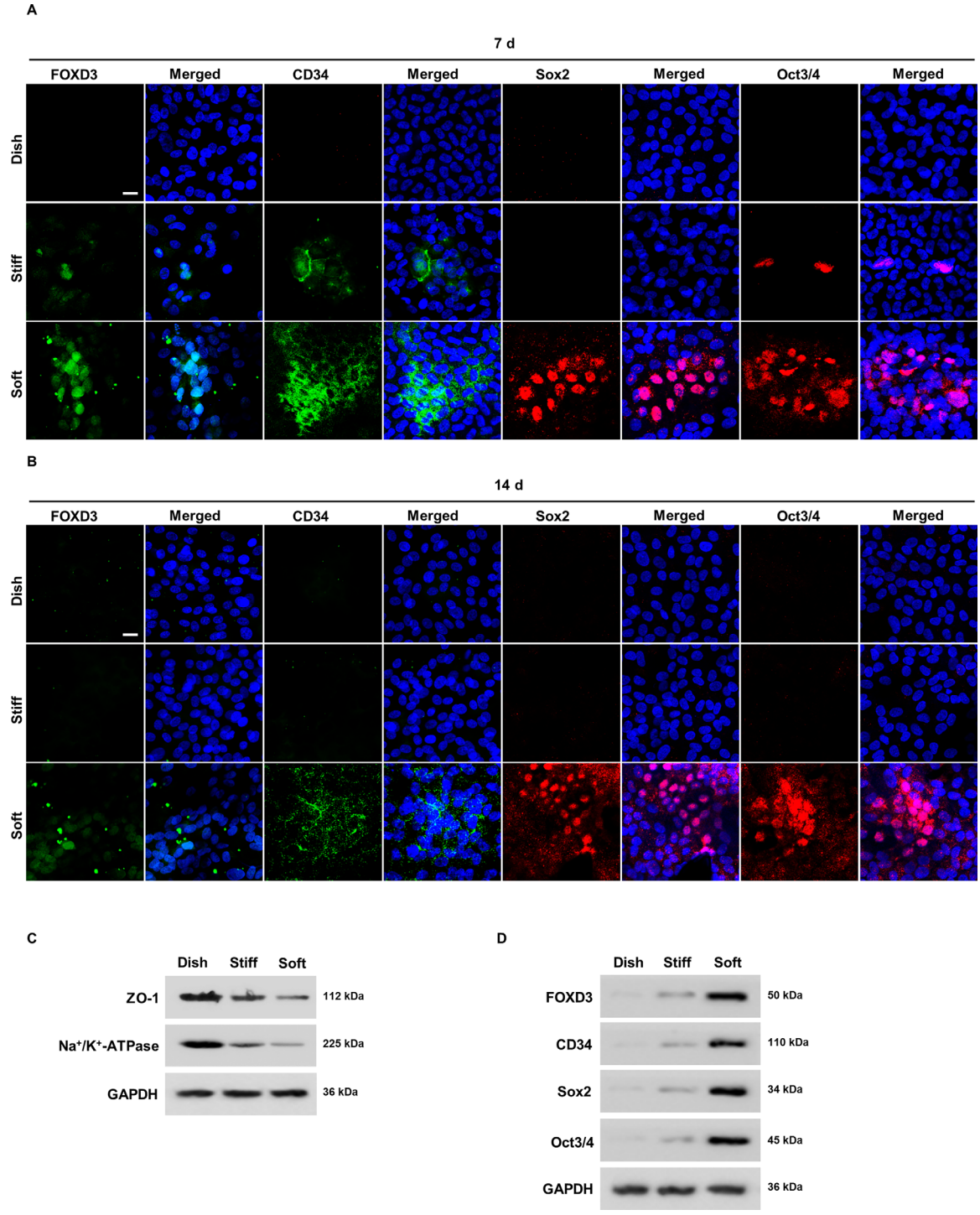

Figure 5. Substrate stiffness regulates the stemness maintenance of CECs in vitro. (**A**) Immunostaining of FOXD3, CD34, Sox2, and Oct3/4 of CECs in dish, stiff, and soft substrates after 7-day culture. (**B**) Immunostaining of FOXD3, CD34, Sox2, and Oct3/4 of CECs in dish, stiff, and soft substrates after 14-day culture. (**C**) Immunoblotting of ZO-1 and Na^+/K^+-ATPase of CECs in dish, stiff, and soft substrates after 7-day culture. (**D**) Immunoblotting of FOXD3, CD34, Sox2, and Oct3/4 of CECs in dish, stiff, and soft substrates after 7-day culture.

Discussion

Accumulating evidence has shown that peripheral CECs are less differentiated than central CECs, which is highly suggestive of the existence of a stem cell niche located at the peripheral corneal endothelium.[8,10,11] The mechanism behind the fate difference of endothelial cells caused by different microenvironments is still unclear. In the study of corneal epithelium and trabecular meshwork cells,[32,33] the effect of the biomechanical microenvironment on cell behavior and stemness regulation has been reported, but there is no relevant research to confirm in corneal endothelial cells. In accordance with other studies,[34,35] our preliminary result confirmed that CECs with high stemness but

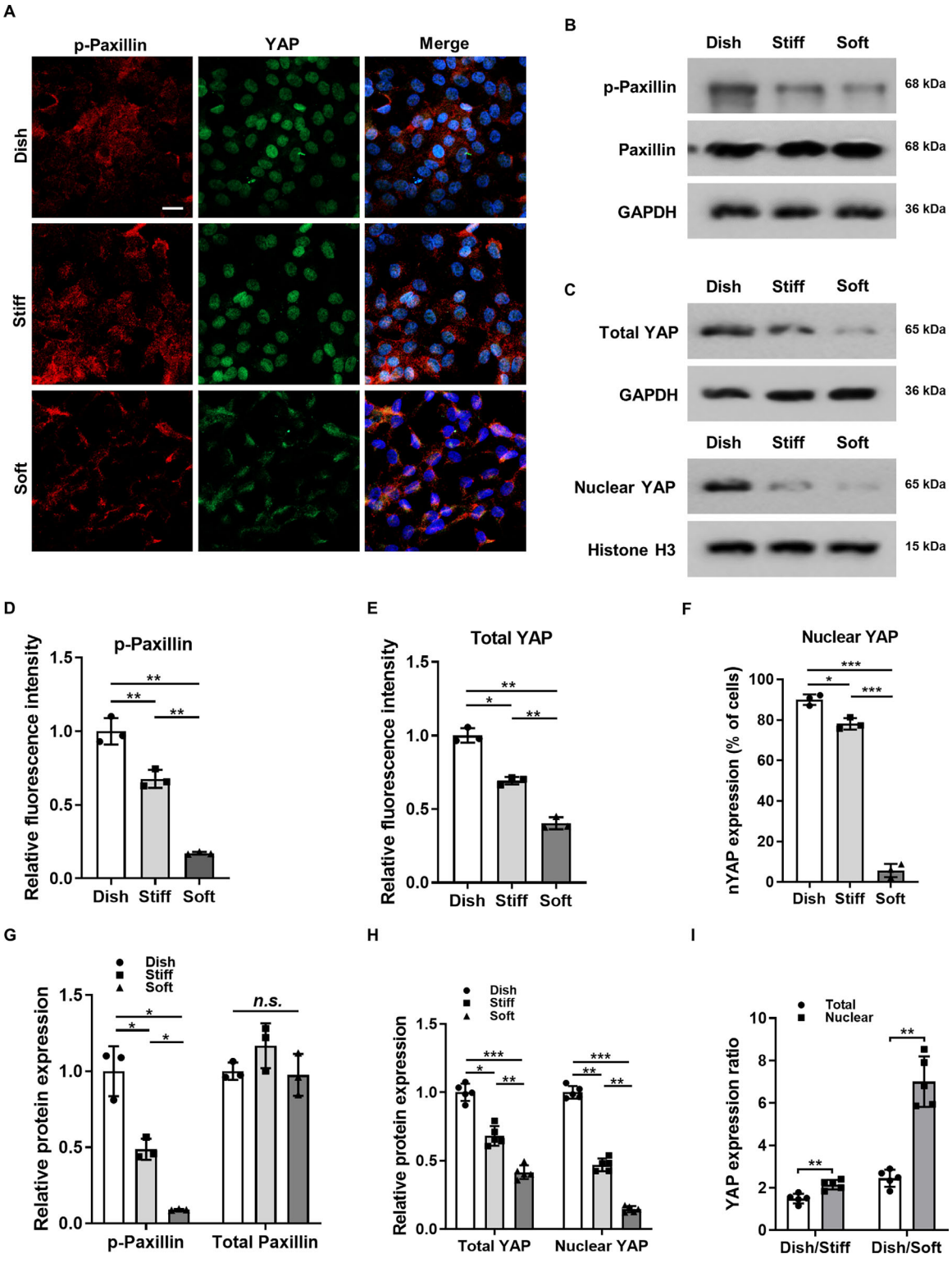

Figure 6. Substrate stiffness modulates the YAP localization in CECs in vitro. (**A**) Immunostaining of phospho-paxillin and YAP of CECs in dish, stiff, and soft substrates. (**B**, **C**) Immunoblotting of phosphor-paxillin, paxillin, total YAP, and nuclear YAP of CECs in dish, stiff, and soft substrates. (**D**, **E**) Relative fluorescence intensity of phosphor-paxillin, total YAP, and nuclear YAP of CECs in dish, stiff, and soft substrates. (**F**) Nuclear YAP expression of CECs in dish, stiff, and soft substrates. (**G**, **H**) Immunostaining of phospho-paxillin, total paxillin, total YAP, and nuclear YAP of CECs in dish, stiff, and soft substrates. (**I**) The total YAP expression ratio of dish/stiff and dish/soft cells and the nuclear YAP expression ratio of dish/stiff and dish/soft cells. Representative images and quantitative data are shown. *Bar graphs* show the statistical analysis of at least three independent experiments. All quantitative data are presented as mean ± SD ($^{*}P < 0.05$, $^{**}P < 0.01$, and $^{***}P < 0.001$). *Scale bar*: 20 µm in (**A**).

Investigative Ophthalmology & Visual Science

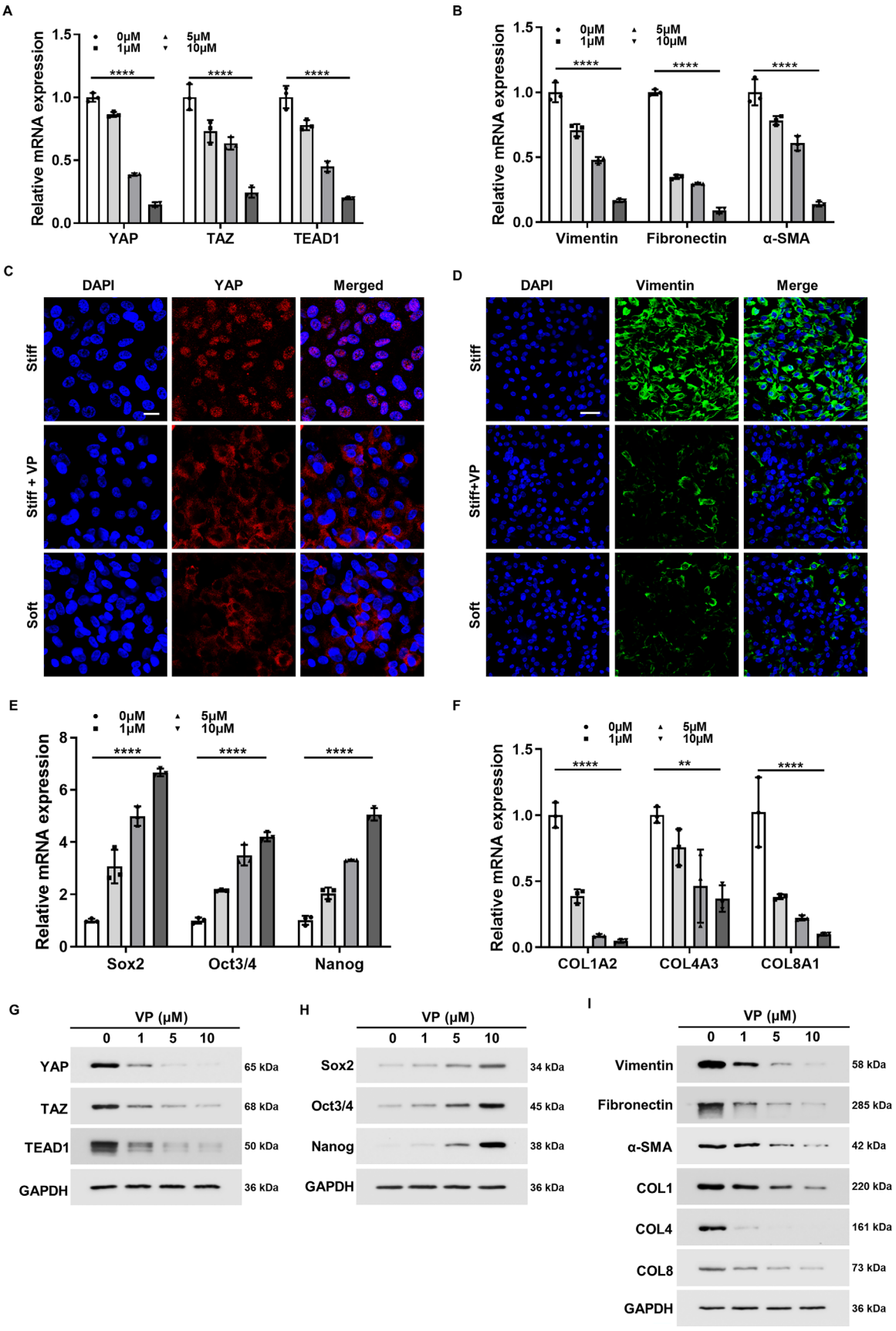

Figure 7. YAP inhibition rescues the stemness loss and EnMT of CECs in vitro. (**A**) The mRNA expression of YAP, TAZ, and TEAD1 in CECs among stiff and verteporfin treated (1, 5, and 10 μM, 48 hours). (**B**) The mRNA expression of vimentin, fibronectin, and α-SMA in CECs among stiff and verteporfin treated (1, 5, and 10 μM, 48 hours). (**C**) Immunostaining of YAP of CECs among stiff and CECs treated

with 5 µM verteporfin for 48 hours in stiff and soft. (**D**) Immunostaining of vimentin of CECs among stiff and CECs treated with 5 µM verteporfin for 48 hours in stiff and soft. (**E**) The mRNA expression of Sox2, Oct3/4, and Nanog in CECs among stiff and verteporfin treated (1, 5, and 10 µM, 48 hours). (**F**) The mRNA expression of COL1A2, COL4A3, and COL8A1 among stiff and verteporfin treated (1, 5, and 10 µM, 48 hours). (**G**) Immunoblotting of YAP, TAZ, and TEAD1 in CECs among stiff and verteporfin treated (1, 5, and 10 µM, 48 hours). (**H**) Immunoblotting of Sox2, Oct3/4, and Nanog in CECs among stiff and verteporfin treated (1, 5, and 10 µM, 48 hours). (**I**) Immunoblotting of vimentin, fibronectin, α-SMA, COL1A2, COL4A3, and COL8A1 in CECs among stiff and verteporfin treated (1, 5, and 10 µM, 48 hours). Representative images and quantitative data are shown. *Bar graphs* show the statistical analysis of at least three independent experiments. All quantitative data are presented as mean ± SD (**$P < 0.01$ and ****$P < 0.0001$). *Scale bar*: 20 µm in (**C**) and (**D**).

low differentiation marker expression reside in the periphery of the cornea. According to previous research reports, the composition, architecture, signaling, and biomechanics of the niche provide the necessary cues regulating cell function in the developing and adult organism.[36,37] In this study, our findings revealed that DM substrate stiffness modulates the stemness maintenance and differentiation of CECs through the paxillin–YAP signal pathway.

Studies have reported that biomechanical changes to DM precede endothelial cell loss in an early-onset murine model of Fuchs endothelial corneal dystrophy.[38] This reveals that biomechanics plays an important role in the behavior regulation of corneal endothelial cells. We used AFM to measure the central and peripheral DM of rabbits and found that the stiffness of the central area was measured to be 14-fold higher than the peripheral area, at 6.88 ± 3.18k Pa compared to 0.49 ± 0.30 kPa (Fig. 3A). Descemet's membrane increases in thickness with age, and the elastic properties may be modulated throughout the life of the individual.[39] In this study, we determined the local stiffness of the central/peripheral region on the same rabbit cornea, which avoiding individual variation and the age interference. The atomic mechanics measurement method we have chosen (improved by probe, etc.) avoids the disturbance of topological structure and stroma substrate on the measurement result. Meanwhile, we conducted acellular treatment on DM, which can also eliminate the interference of corneal endothelial cells on the measurement results.[31] In order to clarify the relationship between substrate stiffness and corneal endothelial cell stemness, we established an in vitro culture model with a different elastic modulus. To imitate the status of peripheral and central DM, elastic moduli of collagen I–coated dish, stiff, and soft substrates were set as 28.15 ± 4.64 kPa, 5.64 ± 1.36 kPa, and 1.65 ± 1.03kPa, respectively. Consistent with the results observed by ex vivo experiment, CECs presented higher stemness but lower differentiation on the softer substrate in vitro model. Collectively, these results suggest that the stiffness in the microenvironment plays an important role in the regulation of the fate of corneal endothelial cells.

As an external signal, mechanical stiffness of the extracellular matrix is capable of governing stem cell fate determination, but how this biophysical cue is translated into intracellular signaling remains elusive. Here, we elucidate mechanisms by which corneal endothelial progenitors respond to microenvironmental stiffness through the dynamics of the cytoskeletal network, leading to changes in gene expression via biophysical transduction signaling pathways in vitro. The transcriptional coactivators YAP and TAZ were recently recognized as key mediators of the biological effects observed in response to ECM elasticity and cell shape.[13] When phosphorylated by large tumor suppressor kinase 1/2 (LATS1/2), YAP/TAZ are localized in the cytoplasm and incapable of binding transcriptional enhanced associate domain (TEAD), thus rendering TEAD transcriptionally inactive. Upon dephosphorylation, YAP/TAZ are translocated to the nucleus to bind TEAD and drive transcription of target genes that are critical for cell growth, proliferation, and survival.[40] Recent studies demonstrated the critical role of YAP signaling in the regulation of mechanosensitive mesenchymal stem cells differentiation.[41] Mascharak et al.[42] reported the necessity of YAP activation in topography-mediated transition of model endothelium toward a highly proliferative and migratory phenotype. Bao et al.[43] demonstrated that cellular volume and matrix stiffness direct stem cell behavior in three-dimensional micro-niches through YAP/TAZ signaling. These studies highlighted the mechanotransducive mechanisms acting upstream of YAP transcriptional activity via Rho GTPases, cytoskeletal contractility, and F-actin mechanics. Our study showed that high-stiffness substrates activated the YAP signaling. This differentiation-associated YAP nuclear translocation was reported in many other types of stem cells and could be likely due to changes in composition of structural ECM proteins. To determine whether YAP localization is regulated by the stiffness of substrate, we investigated the regional expression of YAP and pYAP. Clearly, YAP was mostly located in the nucleus of cells in the stiff substrate, consisting of relatively higher expression of collagen fibrils, while cells in the soft substrate had high levels of phosphorylated and cytosolic YAP. In this study, we identified YAP as a key regulator of corneal endothelial progenitors that maintains stemness and inhibits EnMT in vitro. In the future, further research should be considered on the effect of stiffness on the phenotype of CECs in vivo.

In conclusion, this study demonstrates the strong correlation between substrate stiffness, YAP-dependent mechanotransduction, and endothelial cell phenotype. Specifically, our experiments showed that peripheral DM is softer than central DM, thereby supporting the growth of corneal endothelial progenitors with suppressed YAP signaling, whereas central DM promoted YAP activation while eliciting cell differentiation ex vivo. Moreover, we applied this phenomenon to the development of a collagenase-based method to affect CEC phenotype-through-biomechanical modulation in vitro. Soft substrate enhances the stem cell phenotype of CECs by the mechanosensitive regulation of YAP subcellular expression. This work also provides a mechanism for regulating the expansion of progenitors/stem cells in tissue engineering of corneal endothelial cells.

Acknowledgments

Supported by National Key Research and Development Program of China (2017YFE0103500), National Natural Science Foundation of China (81600708), and Natural Science Foundation of Hubei Province of China (2019CFB152).

Disclosure: **S. Liu**, None; **H. Chen**, None; **H. Xie**, None; **X. Liu**, None; **M. Zhang**, None

References

1. Kabosova A, Azar DT, Bannikov GA, et al. Compositional differences between infant and adult human corneal basement membranes. *Invest Ophthalmol Vis Sci*. 2007;48:4989–4999.
2. LeBleu VS, Macdonald B, Kalluri R. Structure and function of basement membranes. *Exp Biol Med (Maywood)*. 2007;232:1121–1129.
3. Frantz C, Stewart KM, Weaver VM. The extracellular matrix at a glance. *J Cell Sci*. 2010;123:4195–4200.
4. Tuft SJ, Coster DJ. The corneal endothelium. *Eye (Lond)*. 1990;4(pt 3):389–424.
5. Sie NM, Yam GH, Soh YQ, et al. Regenerative capacity of the corneal transition zone for endothelial cell therapy. *Stem Cell Res Ther*. 2020;11:523.
6. Amann J, Holley GP, Lee SB, Edelhauser HF. Increased endothelial cell density in the paracentral and peripheral regions of the human cornea. *Am J Ophthalmol*. 2003;135:584–590.
7. Schimmelpfennig BH. Direct and indirect determination of nonuniform cell density distribution in human corneal endothelium. *Invest Ophthalmol Vis Sci*. 1984;25:223–229.
8. Bednarz J, Rodokanaki-von Schrenck A, Engelmann K. Different characteristics of endothelial cells from central and peripheral human cornea in primary culture and after subculture. *In Vitro Cell Dev Biol Anim*. 1998;34:149–153.
9. Joyce NC. Proliferative capacity of corneal endothelial cells. *Exp Eye Res*. 2012;95:16–23.
10. McGowan SL, Edelhauser HF, Pfister RR, Whikehart DR. Stem cell markers in the human posterior limbus and corneal endothelium of unwounded and wounded corneas. *Mol Vis*. 2007;13:1984–2000.
11. Whikehart DR, Parikh CH, Vaughn AV, Mishler K, Edelhauser HF. Evidence suggesting the existence of stem cells for the human corneal endothelium. *Mol Vis*. 2005;11:816–824.
12. Discher DE, Mooney DJ, Zandstra PW. Growth factors, matrices, and forces combine and control stem cells. *Science*. 2009;324:1673–1677.
13. Koo JH, Guan K-L. Interplay between YAP/TAZ and metabolism. *Cell Metab*. 2018;28:196–206.
14. Panciera T, Azzolin L, Cordenonsi M, Piccolo S. Mechanobiology of YAP and TAZ in physiology and disease. *Nat Rev Mol Cell Biol*. 2017;18:758–770.
15. Nardone G, Oliver-De La Cruz J, Vrbsky J, et al. YAP regulates cell mechanics by controlling focal adhesion assembly. *Nat Commun*. 2017;8:15321.
16. Ross TD, Coon BG, Yun S, et al. Integrins in mechanotransduction. *Curr Opin Cell Biol*. 2013;25:613–618.
17. López-Colomé AM, Lee-Rivera I, Benavides-Hidalgo R, López E. Paxillin: a crossroad in pathological cell migration. *J Hematol Oncol*. 2017;10:50.
18. Hu JK, Du W, Shelton SJ, Oldham MC, DiPersio CM, Klein OD. An FAK-YAP-mTOR signaling axis regulates stem cell-based tissue renewal in mice. *Cell Stem Cell*. 2017;21:91–106.e106.
19. Husari A, Steinberg T, Dieterle MP, et al. On the relationship of YAP and FAK in hMSCs and osteosarcoma cells: discrimination of FAK modulation by nuclear YAP depletion or YAP silencing. *Cell Signal*. 2019;63:109382.
20. Musah S, Morin SA, Wrighton PJ, Zwick DB, Jin S, Kiessling LL. Glycosaminoglycan-binding hydrogels enable mechanical control of human pluripotent stem cell self-renewal. *ACS Nano*. 2012;6:10168–10177.
21. Musah S, Wrighton PJ, Zaltsman Y, et al. Substratum-induced differentiation of human pluripotent stem cells reveals the coactivator YAP is a potent regulator of neuronal specification. *Proc Natl Acad Sci USA*. 2014;111:13805–13810.
22. Gouveia RM, Lepert G, Gupta S, Mohan RR, Paterson C, Connon CJ. Assessment of corneal substrate biomechanics and its effect on epithelial stem cell maintenance and differentiation. *Nat Commun*. 2019;10:1496.
23. Abrams GA, Schaus SS, Goodman SL, Nealey PF, Murphy CJ. Nanoscale topography of the corneal epithelial basement membrane and Descemet's membrane of the human. *Cornea*. 2000;19:57–64.
24. Zhang Y, Hu Z, Qu J, et al. Tissue-engineered corneal endothelial sheets using ultrathin acellular porcine corneal stroma substrates for endothelial keratoplasty. *ACS Biomater Sci Eng*. 2022;8:1301–1311.
25. Liu X, Tseng SC, Zhang MC, et al. LIF-JAK1-STAT3 signaling delays contact inhibition of human corneal endothelial cells. *Cell Cycle*. 2015;14:1197–1206.
26. Zhu Y-T, Tighe S, Chen S-L, et al. Manufacturing of human corneal endothelial grafts. *Ocular Surface*. 2023;29:301–310.
27. Zhu YT, Li F, Han B, et al. Activation of RhoA-ROCK-BMP signaling reprograms adult human corneal endothelial cells. *J Cell Biol*. 2014;206:799–811.
28. Mimura T, Joyce NC. Replication competence and senescence in central and peripheral human corneal endothelium. *Invest Ophthalmol Vis Sci*. 2006;47:1387–1396.
29. Levis HJ, Brown RA, Daniels JT. Plastic compressed collagen as a biomimetic substrate for human limbal epithelial cell culture. *Biomaterials*. 2010;31:7726–7737.
30. Mi S, Chen B, Wright B, Connon CJ. Ex vivo construction of an artificial ocular surface by combination of corneal limbal epithelial cells and a compressed collagen scaffold containing keratocytes. *Tissue Eng Part A*. 2010;16:2091–2100.
31. Thomasy SM, Raghunathan VK, Winkler M, et al. Elastic modulus and collagen organization of the rabbit cornea: epithelium to endothelium. *Acta Biomaterialia*. 2014;10:785–791.
32. Bhattacharya S, Mukherjee A, Pisano S, et al. The biophysical property of the limbal niche maintains stemness through YAP. *Cell Death Differ*. 2023;30:1601–1614.
33. Williams AL, Bohnsack BL. Neural crest derivatives in ocular development: discerning the eye of the storm. *Birth Defects Res C Embryo Today*. 2015;105:87–95.
34. Yam GH, Seah X, Yusoff N, et al. Characterization of human transition zone reveals a putative progenitor-enriched niche of corneal endothelium. *Cells*. 2019;8:1244.
35. Yu WY, Sheridan C, Grierson I, et al. Progenitors for the corneal endothelium and trabecular meshwork: a potential source for personalized stem cell therapy in corneal endothelial diseases and glaucoma. *J Biomed Biotechnol*. 2011;2011:412743.
36. Scadden DT. The stem-cell niche as an entity of action. *Nature*. 2006;441:1075–1079.
37. Burdick JA, Vunjak-Novakovic G. Engineered microenvironments for controlled stem cell differentiation. *Tissue Eng Part A*. 2009;15:205–219.
38. Leonard BC, Jalilian I, Raghunathan VK, et al. Biomechanical changes to Descemet's membrane precede endothelial cell loss in an early-onset murine model of Fuchs endothelial corneal dystrophy. *Exp Eye Res*. 2019;180:18–22.
39. de Oliveira RC, Wilson SE. Descemet's membrane development, structure, function and regeneration. *Exp Eye Res*. 2020;197:108090.
40. Lin KC, Park HW, Guan K-L. Regulation of the Hippo pathway transcription factor TEAD. *Trends Biochem Sci*. 2017;42:862–872.

Investigative Ophthalmology & Visual Science

41. Elosegui-Artola A, Oria R, Chen Y, et al. Mechanical regulation of a molecular clutch defines force transmission and transduction in response to matrix rigidity. *Nat Cell Biol*. 2016;18:540–548.
42. Mascharak S, Benitez PL, Proctor AC, et al. YAP-dependent mechanotransduction is required for proliferation and migration on native-like substrate topography. *Biomaterials*. 2017;115:155–166.
43. Bao M, Xie J, Katoele N, et al. Cellular volume and matrix stiffness direct stem cell behavior in a 3D microniche. *ACS Appl Mater Interfaces*. 2019;11:1754–1759.

Investigative Ophthalmology & Visual Science